

Star formation in the outskirts of DDO 154: A top-light IMF in a nearly dormant disc

Adam B. Watts,^{1*} Gerhardt R. Meurer,^{1†} Claudia D. P. Lagos,¹ Sarah M. Bruzzone,¹, Pavel Kroupa^{2,3}, Tereza Jerabkova^{2,3,4}

¹International Centre for Radio Astronomy Research, The University of Western Australia, Crawley, WA, Australia

²Helmholtz-Institut für Strahlen- und Kernphysik (HISKP), Universität Bonn, Nussallee 14-16, 53115 Bonn, Germany

³Charles University in Prague, Faculty of Mathematics and Physics, Astronomical Institute, V Holešovičkách 2, CZ-180 00 Praha 8, Czech Republic

⁴European Southern Observatory, Karl-Schwarzschild-Straße 2, 85748 Garching bei München

Accepted XXX. Received YYY; in original form ZZZ

ABSTRACT

We present optical photometry of Hubble Space Telescope (*HST*) ACS/WFC data of the resolved stellar populations in the outer disc of the dwarf irregular galaxy DDO 154. The photometry reveals that young main sequence stars are almost absent from the outermost HI disc. Instead, most are clustered near the main stellar component of the galaxy. We constrain the stellar initial mass function (IMF) by comparing the luminosity function of the main sequence stars to simulated stellar populations assuming a constant star formation rate over the dynamical timescale. The best-fitting IMF is deficient in high mass stars compared to a canonical Kroupa IMF, with a best-fit slope $\alpha = -2.45$ and upper mass limit $M_U = 16 M_\odot$. This top-light IMF is consistent with predictions of the Integrated Galaxy-wide IMF theory. Combining the *HST* images with HI data from The HI Nearby Galaxy Survey Treasury (THINGS) we determine the star formation law (SFL) in the outer disc. The fit has a power law exponent $N = 2.92 \pm 0.22$ and zero point $A = 4.47 \pm 0.65 \times 10^{-7} M_\odot \text{ yr}^{-1} \text{ kpc}^{-2}$. This is depressed compared to the Kennicutt-Schmidt Star Formation Law, but consistent with weak star formation observed in diffuse HI environments. Extrapolating the SFL over the outer disc implies that there could be significant star formation occurring that is not detectable in $\text{H}\alpha$. Last, we determine the Toomre stability parameter Q of the outer disc of DDO 154 using the THINGS HI rotation curve and velocity dispersion map. 72% of the HI in our field has $Q \leq 4$ and this incorporates 96% of the observed MS stars. Hence 28% of the HI in the field is largely dormant.

Key words: galaxies: individual (DDO 154) – galaxies: dwarf – galaxies: stellar content – stars: massive – stars: luminosity function

1 INTRODUCTION

The Initial Mass Function (IMF) and the Star Formation Law (SFL), are two empirical relationships that allow us to characterise star formation in galaxies from relatively simple observables. While they are commonly thought to be universal it is important to test these assumptions in extreme environments. The outer disk of the ISM rich, dark matter dominated dwarf irregular galaxy DDO154 provides us with one such extreme environment. The stellar IMF, originally proposed by Salpeter (1955), gives the number density $N(m)$

of new stars of mass m formed in an event as a single slope power law $N(m)dm \propto m^\alpha dm$ with $\alpha = -2.35$. It remains one of the most enduring star formation relationships, and is used in determinations of total star formation rates (SFR) from various tracers such as $\text{H}\alpha$ and ultraviolet emission (e.g. Kennicutt 1989, 1998; Meurer et al. 2009), star formation histories (SFH) from colour magnitude diagrams (CMD) of resolved stellar populations (e.g. Dolphin 2002; Barker et al. 2007; Hillis et al. 2016; Williams et al. 2009a, 2013), total stellar mass estimates from luminosities (e.g. Baldry et al. 2008; Tortora et al. 2010; Taylor et al. 2011; Moffett et al. 2016), and supernova rates (e.g. Barris & Tonry 2006; Mannucci et al. 2008; Scannapieco & Bildsten 2005). Since Salpeter’s original proposal, the IMF has been found to

* E-mail: adam.watts@uwa.edu.au

† E-mail: gerhardt.meurer@uwa.edu.au

turn over below $1 M_{\odot}$ and is commonly parameterised as a broken power law (Kroupa 2001) or log-normal distribution (Chabrier 2003). Theoretically its shape has been shown to be invariant (e.g. Krumholz 2011; Krumholz et al. 2012) or variable (e.g. Bate et al. 2003; Bate & Bonnell 2005; Bonnell 2008; Bertelli Motta et al. 2016) depending on the star-forming conditions, or whether it is integrated over the galaxy (Weidner & Kroupa 2005). Many observations of the Milky Way and Magellanic Clouds have shown little to no evidence of variations outside statistical uncertainties (e.g. Freedman 1985; Scalo 1985; Phelps & Janes 1993; Elmegreen 1999; Bastian et al. 2010), which has led to the assumption of a universal IMF (Scalo 1986; Kroupa 2001; Chabrier 2003).

The universality of the IMF has become a hotly debated topic as an increasing number of observational studies have provided evidence of real, detectable variations (e.g. Cappellari et al. 2012; Davis & McDermid 2017; Kalari 2017; Romano et al. 2017; Schneider et al. 2018). A non-universal high mass slope ($m > 1M_{\odot}$, from here just ‘slope’) has been invoked to explain high mass to light ratios in low mass galaxies, deficiencies of H α emission, and high x-ray emission from ultra compact dwarf galaxies (Hoversten & Glazebrook 2008; Lee et al. 2004, 2009; Pflamm-Altenburg et al. 2007; Meurer et al. 2009; Dabringhausen et al. 2010). These phenomena are thought to be caused by an IMF that varies with star formation intensity, galactocentric radius, metallicity and local gas density (Gunawardhana et al. 2011; Meurer et al. 2009; Marks et al. 2012). There is also evidence for a varying IMF at masses $m < 1M_{\odot}$ in early type galaxies that could correlate with metallicity and velocity dispersion (La Barbera et al. 2015; Conroy & van Dokkum 2012; Vaughan et al. 2016; Martín-Navarro et al. 2015), and in local group dwarf galaxies (e.g. Geha et al. 2013; Kalirai et al. 2013; Gennaro et al. 2018).

In most studies of resolved stellar populations in nearby galaxies it is common to derive the SFH from the CMD by assuming an IMF (e.g. Geha et al. 1998; Harris & Zaritsky 2004, 2009; Barker et al. 2007; Cignoni et al. 2012; Weisz et al. 2011, 2013, 2015), but if the IMF is not universal, rather steeper or deficient in high mass stars, the SFH could be inferred to be halted or declining when the SFR is actually constant (Meurer et al. 2009). Here we extend the method of Bruzese et al. (2015, hereafter B15) to use the less common approach of deriving the IMF of a stellar population by assuming a plausible form of the SFH. The IMF is thought to show variation in extreme environments such as the extended HI discs of gas rich star-forming galaxies. These regions have low gas and stellar surface densities with correlated diffuse UV emission indicative of low intensity star formation (Thilker et al. 2005, 2007), thought to be deficient in high mass stars (Elmegreen 2004). There are competing models for the deficiency of high mass stars in low density regions: stochasticity of a universal IMF (e.g. Koda et al. 2012), or a varying IMF (e.g. B15).

One model for a varying IMF is the integrated galaxy IMF (IGIMF, e.g. Pflamm-Altenburg et al. 2009). Where many theories adopt a model for star formation where stars can form anywhere, the IGIMF theory restricts star formation to the formation of embedded star clusters. Stars form adhering to a universal form of the IMF but with the up-

per mass limit of each cluster set by its mass, while the clusters form with a consistent cluster mass function whose maximum mass is set empirically by the SFR of the galaxy (Weidner & Kroupa 2005, 2006). According to this theory, the galaxy-wide IMF is top-light for galaxies with a small SFR and top heavy at large SFR (Yan et al. 2017). Thus, the low stellar and gas densities found in the outer discs of galaxies provide an interesting extreme environment for probing the nature of the IMF, and how it may vary with star formation intensity.

The correlation between gas density and SFR density was first proposed by Schmidt (1959) as a power law in volumetric gas density $\rho_{\text{SFR}} \propto \rho_{\text{gas}}^n$ and predicted theoretically that $n = 1.5$. It is commonly expressed in terms of the projected quantities $\Sigma_{\text{SFR}} = A \Sigma_{\text{gas}}^N$, which are more easily measured. Kennicutt (1998) studied this correlation over a range of star-forming conditions with H α derived SFRs and HI + molecular (H $_2$) gas estimates, determining $N = 1.4 \pm 0.15$ and $A = (2.5 \pm 0.7) \times 10^{-4} M_{\odot} \text{ yr}^{-1} \text{ kpc}^{-2}$. This became the canonical ‘Star Formation Law’ (SFL). However, recent determinations on both local and global scales have produced both steeper and flatter values of N (e.g. Momose et al. 2013; Roychowdhury et al. 2015). Almost linear values of N have been determined in the bright centres of galaxies where SFR is more strongly correlated with H $_2$ surface density (e.g. Bigiel et al. 2008; Leroy et al. 2008, 2013; Pflamm-Altenburg & Kroupa 2008, 2009), but in the HI dominated, extended outer discs of spirals and low mass dwarf galaxies SFR correlates strongly with the HI surface density and N is characteristically steeper, while molecular gas is undetectable (e.g. Bigiel et al. 2008, 2010; Wyder et al. 2009; Dessauges-Zavadsky et al. 2014; Wang et al. 2017). There are some empirically proposed complications to the SFL: such as truncated star formation due to disc stability (Kennicutt 1989; Martin & Kennicutt 2001), and a SFL that depends on both the stellar and ISM mass densities (Ryder & Dopita 1994; Dopita & Ryder 1994; Wang et al. 2017).

The theoretical models of Ostriker et al. (2010) and Krumholz (2013) suggest the scatter observed in determinations of N in HI dominated regions could be explained by a H $_2$ gas density that is sensitive to other parameters such as metallicity and stellar and dark matter density. Determining the SFL in the outer discs of galaxies gives us a unique way of comparing these models to observations.

In this work we constrain the IMF and SFL in the extended HI outer disc of the local dwarf irregular galaxy DDO 154, using data from the Hubble Space Telescope and the Very Large Array. DDO154 is one of the most gas rich galaxies known, harbouring a HI disc that extends to ~ 6 times the Holmberg radius¹ (Kennicutt & Skillman 2001). Despite being so gas rich, its SFR is typical of those observed for dwarf irregular galaxies implying the star formation efficiency (SFE) is low (Kennicutt & Skillman 2001). Mass modelling of DDO 154 reveals a mass to light ratio (M_T/L_B) of 80, corresponding to a 90% dark matter content, making it also one of the ‘darkest’ disc galax-

¹ DDO154 is projected on the sky 5.1 arcmin NW of the background Coma cluster galaxy NGC4789 (see Fig. 1), hence it is also catalogued as NGC489A.

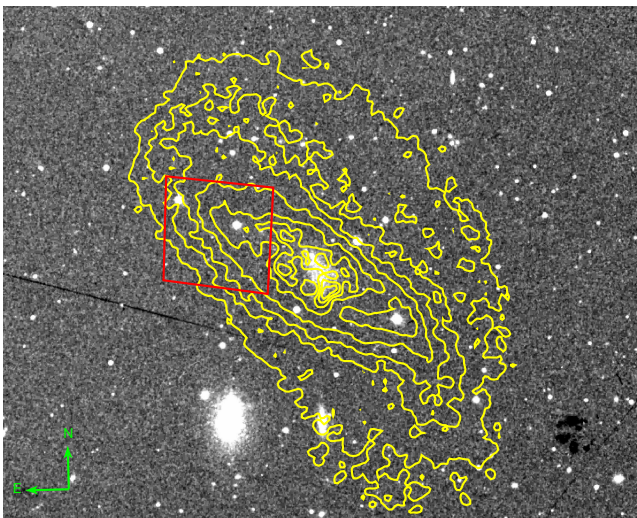


Figure 1. Palomar Observatory Sky Survey 103aE (red) digitised photograph of DDO 154 showing the central low surface brightness optical component of the galaxy with the *HST*/ACS footprint overlaid in red. The image covers an area of $22' \times 16.5'$. Contours of HI mass surface density from THINGS (Walter et al. 2008) are overlaid in yellow at densities of 0.1, 0.5, 1, 2, 4, 6, 8, and $10 M_{\odot} \text{pc}^{-2}$.

Table 1. Adopted properties for DDO 154

Parameter	Value	Reference
Metallicity (Z)	$0.1 Z_{\odot}$	Kennicutt & Skillman (2001)
Distance (Mpc)	4.02	Jacobs et al. (2009)
Environment	Isolated	Karachentsev et al. (2004)
Pixel Scale (pc/pix)	0.974	-
$E(B - V)^G$ (mag)	0.009	Jacobs et al. (2009)
Inclination	66°	Walter et al. (2008)
Position Angle	229.7°	de Blok et al. (2008)
V_{hel} (km s^{-1})	374	Karachentsev et al. (2013)
M_{HI} ($10^7 M_{\odot}$)	39.4	Carignan & Purton (1998)
M_B (Mag)	-13.92	Karachentsev et al. (2013)
M_T/L_B	80	Kennicutt & Skillman (2001)
M_{\star} ($10^7 M_{\odot}$)	1.26	Leroy et al. (2008)
SFR ($\text{H}\alpha$, $10^{-3} M_{\odot} \text{yr}^{-1}$)	2.79 ± 0.56	Kennicutt & Skillman (2001)
SFR (UV + IR, $10^{-3} M_{\odot} \text{yr}^{-1}$)	5	Leroy et al. (2008)

ies known (Carignan & Freeman 1988; Carignan & Purton 1998; de Blok et al. 2008). Since its nearest known neighbours are > 350 kpc away (Carignan & Purton 1998) tidal interactions (i.e. external triggers) are not a likely cause for these extreme properties nor for any postulated recent fluctuations in its star formation rate. This makes it a valuable candidate for investigating the SFL and variations in the IMF, and Table 1 lists the adopted parameters for DDO 154 and their source. We adopt the upper mass limit of $M_U = 120 M_{\odot}$ and high mass slope $\alpha = -2.35$ as the standard IMF and refer it to as the Kroupa IMF (Kroupa 2001). This paper is organised as follows. In §2 we present our data and photometry. In §3 we describe our modelling of the CMD and statistical testing of it, and in §4 we present our results constraining the IMF. In §5 we determine the SFL in DDO154 and investigate the stability of the gas disc, and in §6 we conclude.

2 DATA AND ANALYSIS

2.1 HST images

We use data from the Advanced Camera for Surveys (ACS) Wide Field Camera (WFC) of the Hubble Space Telescope *HST* (proposal ID:10287). The observations consist of three exposures in the F475W (g_{475}), F606W (V_{606}), and F814W (I_{814}) filters with combined exposure times of 1800, 1800, and 3433 seconds respectively. The observations focus on the extended outer disc centred on R.A.: $12^{\text{h}} 54^{\text{m}} 19.9^{\text{s}}$, Dec: $+27^{\text{d}} 10.2^{\text{m}} 11.2^{\text{s}}$ (J2000), shown in Fig. 1, 5.71 kpc from the centre of the galaxy and covering radii between 98 – 340 arcsec (2.3 – 12.2 kpc, corrected for inclination and position angle).

2.2 Photometry

We perform PSF photometry using DOLPHOT, a modified version of HSTphot designed specifically for ACS/WFC images (Dolphin 2000). Preprocessing is done using the DOLPHOT routines *acsmask*, *splitgroups* and *calcsky* to apply the pixel masks, separate the two ACS chips, and produce robust sky images respectively. We follow the method of B15 and adopt the recommended parameter file from the DOLPHOT ACS user manual with changes to a few select parameters as suggested by Dalcanton et al. (2009). We set the photometry parameters *FitSky*, *RAper* and *Force1* to their recommended values as they were found to have the greatest effects on the quality of the photometry. DOLPHOT outputs all detected objects with positions on the reference image and magnitudes in the VEGAMAG system calculated using the transforms of Sirianni et al. (2005) and corrected for CTE loss following Riess & Mack (2004). We use the photometric quality parameters roundness, sharpness, crowding, and signal to noise (S/N) provided for each star in each filter to clean the catalogue of non-stellar detections, adopting the same quality cuts as B15 and Dalcanton et al. (2009). To make the final photometric catalogue stars must satisfy $(S/N)_{1,2} \geq 4$, $|\text{sharp}_1 + \text{sharp}_2| < 0.05$, $(\text{crowd}_1 + \text{crowd}_2) < 0.6$, and $|\text{round}_1 + \text{round}_2| < 1.4$ where the subscripts (1,2) denote one of the filter pairs (g_{475}, V_{606}) or (V_{606}, I_{814}). Satisfying the conditions in at least one filter pair was sufficient to be included in the final photometric catalogue. The final catalogue consisted of 2698 stars out of the 173 112 in the original DOLPHOT output.

2.3 Artificial star tests

To quantify photometric uncertainties and the completeness of the CMDs we ran artificial star tests using DOLPHOT (similar to the work of Dalcanton et al. 2012 and B15). The inserted and recovered magnitudes of these stars determines how well objects of known magnitude and colour are recovered by DOLPHOT. We simulated 300,000 artificial stars with colour and magnitude limits set by the observed data, distributed uniformly over the images as crowding is low in the outer disc. The colour limits were defined using the g_{475} and I_{814} bands since they provide the largest colour baseline and we account for scatter due to photometric uncertainties ($-1 \leq g_{475} - I_{814} \leq 3$ and $20 \leq g_{475} \leq 29$). This produces a

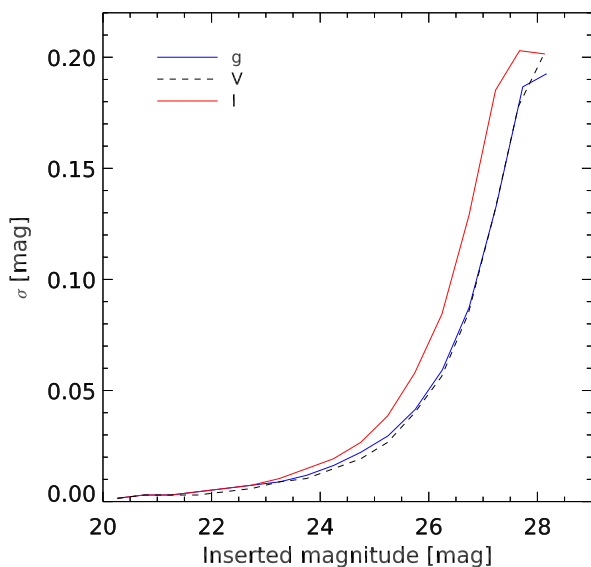


Figure 2. Median photometric uncertainties derived from artificial star tests.

catalogue of the artificial stars with their inserted and recovered magnitudes, positions, and quality parameters to which we applied the same quality cuts. Using Gaussian statistics the median absolute deviation between the inserted and recovered magnitude of stars in 0.5 mag bins is calculated to quantify the photometric uncertainties, which we show in Fig. 2 as a function of inserted magnitude. The completeness of the CMD is quantified by comparing the ratio of the number of surviving to inserted artificial stars as a function of position of the CMD using bins of 0.25 mag and 0.5 mag in colour and magnitude respectively. The cyan completeness contour in Fig. 3 marks the region of the CMD below which less than 60% of inserted artificial stars are recovered in the same bin. The features of the CMD we are interested in are above this contour, and so only mildly affected by incompleteness. We use the photometric uncertainties and completeness map to correct our stellar population models and account for these effects.

2.4 Final photometric catalogues

The CMDs shown in Fig. 3 reveal the different populations present in the outer disc of DDO 154. Aside from the red giant branch stars, which formed between 1 and 10 Gyr ago, the most prominent feature is the vertical sequence of stars rising around colour ($g_{475} - I_{814}$) = 0. This is a mixture of young main sequence (MS) stars and older, lower mass helium burning ‘blue loop’ (BL) stars (Dalcanton et al. 2012). As these stars could contaminate our MS selection, we take careful considerations to avoid them. The largest colour separation is provided by the ($g_{475} - I_{814}$) colour CMD, better disentangling the bluer MS stars from the redder BL stars. This is supported by the evolutionary tracks shown in Fig. 3: the thicker part of the tracks (MS phase) is consistent with the bluer portion of the vertical sequence, while the redder half is consistent with vertex of the tracks migrating left after the RGB phase. Considering the photometric

uncertainties we separate the two populations using the selection boxes shown in Fig. 3 to minimise contamination from BL stars. There are 162 MS stars in our selection box, the faintest of which roughly corresponds to the MS turn-off luminosity of a $\sim 4 M_{\odot}$ star.

In the right panel of Fig. 4 we plot the spatial distribution of the stars, colour coded by their evolutionary phase. The RGB stars, aside from some clustering near the main stellar disc at the bottom of the image, are distributed relatively uniformly over the field. The MS and BL stars have a similar but noticeably more clumpy distribution. This is shown in the right panel of Fig. 4 where we plot the disk-plane radial distribution of stars in bins of 0.5 kpc. The surface density of RGB stars shows a gradual decline with radius, whereas the MS and BL stars show a sharper decline. Aside from one small association not far from the main stellar component, there are almost no MS or BL stars in the extended outer disc, implying recent star formation is almost absent. This association (hereafter ASN-1) is marked in the left panel of Fig. 4 with a red circle and is located at R.A.: $12^h 54^m 18.4^s$, Dec: $+27^d 9^m 41.3^s$ (J2000), which is 5.58 kpc from the centre. It has a maximum radius of ~ 195 pc, and contains 6 MS stars and 2 BL stars.

2.5 Comparisons to GALEX UV images

As the stars in our MS selection box are more massive than $4M_{\odot}$ (i.e. B and O stars) we should observe emission in the UV detectable by the GALEX satellite. In Fig. 5 we compare the locations of the MS stars to NUV images of DDO 154. The majority of the UV emission is located near the main stellar disc. There is good correlation between the MS stars and UV emission, but some stars are too faint or sparsely distributed to be detected by GALEX. Of the MS stars at $R > 5$ kpc only ASN-1 shows correlated UV emission.

3 STELLAR POPULATION MODELS

3.1 Star formation history

Either a recent drop in the SFR (a ‘‘gasp’’ in star formation) or a deficiency of high mass stars in the IMF may cause a deficiency of bright blue stars. Thus the IMF and SFH are degenerate; we cannot use our data to solve for both (Miller & Scalo 1979). Here we select a sensible form for the SFH to break this degeneracy and infer the IMF from our data. Star formation in dwarf irregular galaxies is commonly assumed to be continuous and low level, with intermittent bursts (Gerola et al. 1980) triggered by gaseous inflow or interactions (Taylor et al. 1993, 1995). Starbursts are commonly assumed to be short lived, with timescales as short as a few Myr (Ferguson & Babul 1998; Tremonti et al. 2001; Harris et al. 2004), but recent observations have shown that star formation can be significantly elevated on whole-galaxy scales over ~ 100 Myr to Gyr timescales (McQuinn et al. 2010a,b, 2012). This agrees with crossing time arguments where the duration of star formation should not be shorter than the time it would take a disturbance (such as a supernova explosion) to cross the star-forming region and quench further star formation (Meurer 2000). This essentially restricts the rapid quenching of star formation to local scales

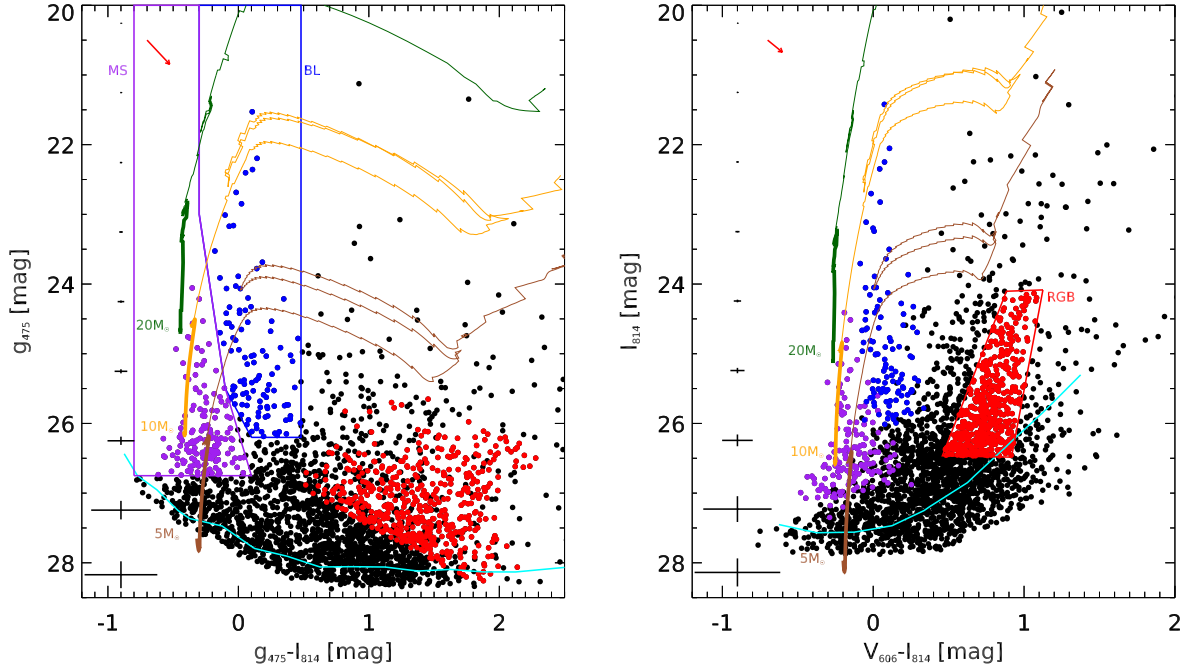


Figure 3. CMDs of the stars recovered from the *HST* ACS/WFC images in g_{475} vs. $(g_{475} - I_{814})$ (left) and I_{814} vs. $(V_{606} - I_{814})$ (right). Error bars on the left show photometric uncertainties and the cyan lines show the 60% completeness limit derived from artificial star tests. PARSEC evolutionary tracks (Bressan et al. 2012; Rosenfield 2016) for 5, 10, and $20 M_{\odot}$ evolutionary tracks are shown in brown, orange and dark green respectively with thicker sections corresponding to the MS phase. The red arrow in the top left of each CMD corresponds to the reddening $E(B - V) = 0.1$, ten times the adopted value for DDO 154. The $g_{475} - I_{814}$ (left) CMD shows the MS and BL selection boxes in purple and blue respectively. The $V_{606} - I_{814}$ CMD (right) outlines the RGB selection box in red. Stars in the MS, BL and RGB selection boxes are coloured purple, blue, and red respectively in both panels.

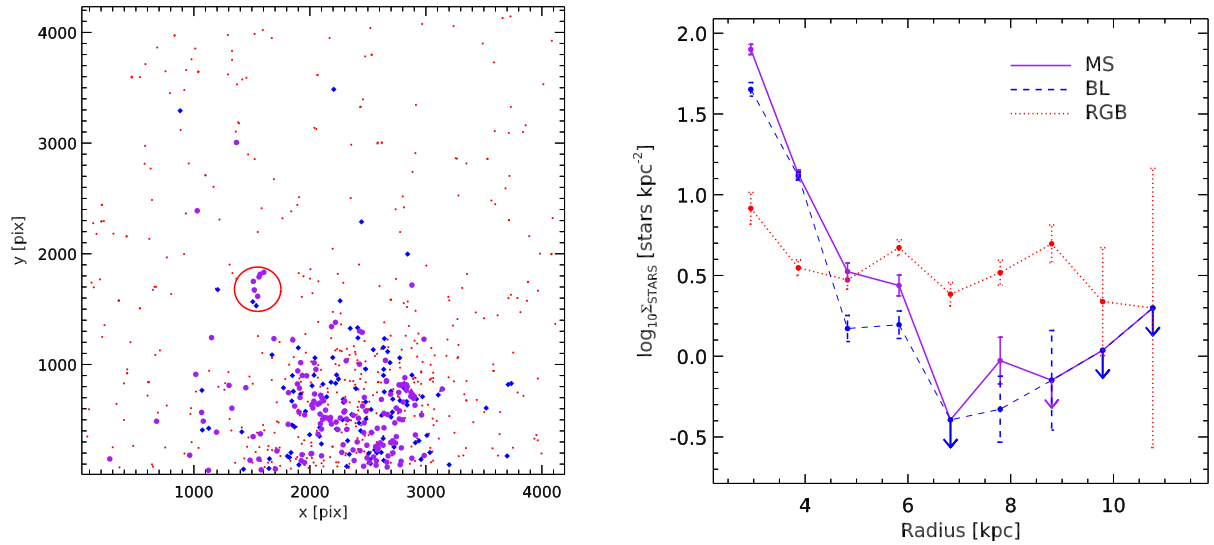


Figure 4. (Left) Spatial distribution of recovered stars in the *HST* images. RGB stars are shown in red, MS stars in purple, and BL stars as blue diamonds. (Right) Disk-plane radial distribution of MS (purple), BL (blue, dashed) and RGB (red, dotted) stars. Error bars correspond to the uncertainty calculated from Poisson statistics, and downward arrows denote upper limits of $1/\text{Area}$ for empty radial bins.

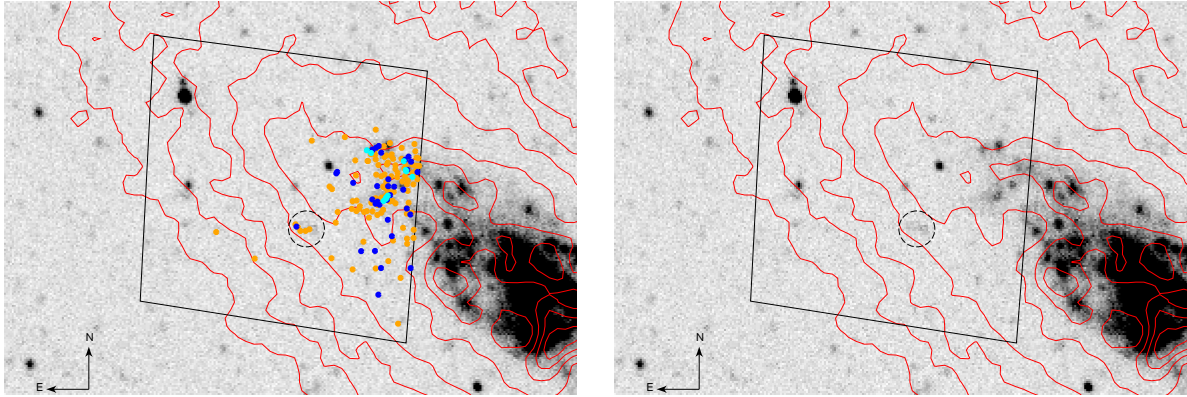


Figure 5. Comparison between the GALEX NUV image and the location of MS stars detected in the *HST* images of the outer disc of DDO 154. Stars with $g_{475} \geq 26$ mag are shown in orange, $26 < g_{475} \leq 25$ mag in blue, and $g_{475} < 25$ mag in cyan. We include images with (left) and without (right) MS detections to reduce crowding and make the NUV emission clearer. The *HST* footprint is shown in black, and the image orientation is shown by the compass in the bottom right corner. Some individual stars appear to show no correlated detection in GALEX, and faint emission can be seen associated with ASN-1 marked by the dashed circle. The brightest NUV sources in the field of view with no correlated MS star detection are foreground stars.

while the global SFR of the galaxy remains elevated and constant. Star formation rates elevated on Gyr timescales have been produced in controlled, non-cosmological simulations of low mass galaxies (e.g. Verbeke et al. 2014; Watts & Bekki 2016). Cosmological zoom-in simulations have produced dwarf galaxy SFHs consisting of consecutive bursts that are effectively constant over Gyr timescales (e.g. Oñorbe et al. 2015), and centrally concentrated ~ 5 to ~ 50 Myr duration bursty SFHs with longer periods of quiescence (e.g. Sparre et al. 2017).

DDO 154 is an isolated galaxy (Karachentsev et al. 2004; Read et al. 2017), its nearest neighbours are NGC 4826 and UGC 7698, both with projected distances greater than 350 kpc away (Carignan & Purton 1998) indicating there has been no recent external triggers capable of creating a starburst. It is undergoing low intensity star formation, harbouring several small HII regions in its main stellar component. The combined $H\alpha$ equivalent width from spectrophotometry is 31 ± 6 (Kennicutt & Skillman 2001) and most of its stellar mass is thought to have been built up by this low intensity star formation. At the current UV+IR SFR of $5 \times 10^{-3} M_{\odot} \text{ yr}^{-1}$ (Leroy et al. 2008) it would take 2.52 Gyr to build the estimated stellar mass of DDO 154 ($1.26 \times 10^7 M_{\odot}$, Leroy et al. 2008). We are not concerned with the central parts of the galaxy, but instead the extended outer disc where DDO 154 shows increasing disk stability, especially beyond $R = 5$ kpc (Meurer et al. 2013). This may mean it is harder for gas clouds to collapse and stars to form.

The MS stars in our images span the majority of the field of view so the minimum timescale we would expect star formation to have lasted would be the crossing time of the ACS/WFC images. Assuming stars are travelling at the typical HI velocity dispersion of 8.62 km s^{-1} (the mean value interior to the radius of 7.5 kpc in our *HST* field of view), this corresponds to an image crossing time of 462 Myr. The lowest mass MS star in our selection box is $4 M_{\odot}$ which has a MS lifetime of 160 Myr (Schaerer et al. 1993) making this the longest timescale we are sensitive to. As the crossing timescale estimate is over twice this

MS lifetime, a constant SFR is a reasonable assumption. We also consider the possibility of a declining SFR due to the consumption of gas based on the model of Kennicutt (1998), where the SFR decreases by 10% each dynamical timescale. The centre of our *HST*/ACS images is 5.71 kpc from the centre of the galaxy, which using the THINGS rotation curve (de Blok et al. 2008) corresponds to $v_{\text{circ}} = 47.2 \text{ km s}^{-1}$. Assuming circular orbits, the orbital time is 743 Myr and dynamical time 242 Myr, corresponding to a 6.7% decrease in SFR over the lifetime of a $4 M_{\odot}$ star. B15 investigated declining star formation rates of similar magnitude and timescale, and found them to produce results effectively equivalent to a constant SFR.

In addition to temporal variations in the formation of stars; their formation environment could also play a role in variations in the high mass end of the IMF. There are two competing models for the formation of high mass stars: competitive accretion and monolithic collapse. In the competitive accretion model (e.g. Bonnell & Bate 2002) high mass stars are formed through interactions between protostars and the accretion of gas in dense environments. This restricts their formation to star clusters where densities are high. The collapse model (e.g. Yorke & Sonnhalter 2002) determines the formation of high mass stars from the properties of the parent molecular cloud and allows high mass stars to form anywhere. Following the review of Lada & Lada (2003) it is commonly assumed that star formation is restricted to clusters, however this assumption may not be valid in low density environments. The review of Krumholz (2014) notes that the fraction of stars formed in clusters depends strongly on the density thresholds used to define them (cf. Bressert et al. 2010). The broad range of densities in which protostars are found neither excludes nor rules out star formation occurring only in clusters (Gieles et al. 2012). However, the models of Kruijssen (2012) indicate that low density star-forming environments should not contribute significantly to bound star formation. Gutermuth et al. (2011) showed that the formation of protostars over large ranges in gas column density shows no distinct break between clus-

ter and field population (cf. Megeath et al. 2016). While Stephens et al. (2017) find that there are no truly isolated O stars in the Magellanic Clouds, and Wright & Mamajek (2018) show OB associations with substructures, Elmegreen (2008) suggested that O and B stars form in loose associations rather than bound clusters in low gas pressure environments. At higher star formation intensities, Meurer et al. (1995) and Larsen & Richtler (2000) have shown that $\sim 20\%$ of the UV light from starburst galaxies comes from young compact star clusters, with a smaller contribution at lower star formation intensity, consistent with other observations (Bressert et al. 2010) and models (Kruijssen 2012) that find $\lesssim 35\%$ of stars form in dense bound clusters. This implies that the formation of bound star clusters should not be prevalent in low density regions such as the outer disc of DDO 154.

As the simplest approach we modelled the outer disc of DDO 154 as random sampling of the IMF and a constant SFH over the dynamical timescale without clustering in space or time.

3.2 Simulated CMDs

To constrain the IMF we compare the main sequence luminosity function (MSLF) of the stellar population in DDO 154 to our simulations. Model CMDs are created by randomly distributing 500,000 stars over an adopted IMF with a constant SFR over 400 Myr. The simulation time is selected to be longer than the MS lifetime of the lowest mass star in our selection box (160 Myr) to account for lower mass stars that could be scattered into the selection box by photometric uncertainties. A lower mass limit of $2.5 M_{\odot}$ is selected to ensure the simulated CMD matches observations as closely as possible and to account for the photometric scattering of fainter stars into the selection box. We adopt the common assumptions for modelling a resolved stellar population: stars are non-rotating, have zero binary fraction, and a uniform metallicity and dust extinction (e.g. Annibali et al. 2013; Hillis et al. 2016; Sacchi et al. 2016). We explore the limitations of these assumptions in §4.3.

The metallicity $Z = 0.0013$ is estimated from the Oxygen abundance $12 + \log(O/H) = 7.67 \pm 0.05$ (Kennicutt & Skillman 2001) using the Asplund et al. (2009) abundance scale, and is approximately 10% of the Solar value. We use the PARSEC interpolated evolutionary tracks (Bressan et al. 2012; Rosenfield 2016) with metallicity $Z = 0.001$ (closest to our adopted value) covering the mass range $1 < m/M_{\odot} < 120$ and evolution of stellar properties from the pre-MS to the end of the asymptotic giant branch. We interpolate between evolutionary tracks for the effective temperature (T_{eff}) and surface gravity ($\log g$) of each star based on its initial mass and age at the end of the simulation. Synthetic photometry is created from the available grid of ATLAS9 spectra (Castelli & Kurucz 2004) using PYSYNPHOT, and interpolated to the T_{eff} and $\log g$ values of the simulated stars. Stars in the pre-MS phase or those too old to be covered by the evolutionary tracks are flagged and removed as they do not meaningfully contribute to the areas of the CMD we are interested in. The model photometry was corrected to the distance and foreground Galactic dust content (Table 1). Photometric uncertainties are modelled by perturbing magnitudes by a Gaus-

sian random variate with a mean set by the star's magnitude and standard deviation set by the median absolute deviation calculated from artificial star tests (§2.3, Fig. 2). Completeness of the CMD is modelled by employing a survival analysis where stars are randomly removed using the fractional completeness map produced from the artificial star tests (§2.3). The simulated populations were created in a grid of two parameters; the IMF upper mass limits $M_U/M_{\odot} = 10, 16, 20, 30, 40, 50, 60, 70, 80, 90, 100, 120$ and high mass slopes $-3.95 \leq \alpha \leq -1.95$ in steps of 0.1. An ensemble of 100 simulated populations are created for each pair of IMF parameters (M_U, α) to measure stochastic effects, and determine more robust mean results.

4 MS LUMINOSITY FUNCTION CONSTRAINTS ON THE IMF

4.1 Best-fitting IMF

We use the two sided Kolmogorov-Smirnov (KS) test to compare the cumulative distribution function (CDF) of the g_{475} band MSLF of the outer disc of DDO 154 to the CDF of stars randomly selected from our simulated stellar populations, as previously done by B15. The number of simulated stars in our MS selection box varies, depending on the IMF parameters, between ~ 1400 ($\alpha = -3.95, M_U = 10 M_{\odot}$) to ~ 4300 ($\alpha = -1.95, M_U = 16 M_{\odot}$). We randomly select N simulated stars from each simulation for comparison where N is a random variate drawn from a Poisson distribution with a mean equal to the number of observed MS stars (162). The KS test parameter D , which represents the maximum deviation between the CDFs of the observations and simulations, is averaged over the 100 simulations for each point in the (M_U, α) parameter space. The simulation set with the minimum D_{ave} is then taken to be the best-fitting pair of IMF parameters.

Fig. 6 shows the distribution over the parameter space D_{ave} values as a contour plot. The best-fitting IMF parameters are $\alpha = -2.45$ and $M_U = 16 M_{\odot}$ which are referred to as the best-fitting IMF from here. There is an extended region of local minima spanning $16 < M_U/M_{\odot} < 120$ implying the upper mass limit is not well constrained. Fig. 7 compares the cumulative MSLF of the observed population (black) to the 20 best-fitting simulated populations from both a Kroupa IMF (blue) and best-fitting IMF (red). Each simulated MSLF was produced using N randomly selected stars, where N is drawn from a Poisson distribution with mean of 162. The best-fit parameters clearly match the observed data better than a Kroupa IMF for a stellar population with a constant SFH over the dynamical timescale. If the Kroupa IMF was a good prescription for star formation in the outer disc of DDO 154, we would expect $\sim 10\%$ ($\sim 1\%$) of stars to be brighter than $g_{475} \sim 24.8$ (23.3) mag. Instead, the observed population shows $\sim 10\%$ ($\sim 1\%$) of stars brighter than $g_{475} \sim 25.3$ (24.2) mag. Hence if stars were forming in the outer disk with a Kroupa IMF, we would see relatively more at brighter magnitudes. Table 2 shows the KS test results between the observed MSLF and the Kroupa and best-fitting IMF averaged over the 100 simulated stellar populations, and the results of the single best-fitting simulation from each IMF. The D_{ave} value disfavors the Kroupa IMF which yields a $p = 0.088$ significance level.

Table 2. KS test maximum deviation (D) averaged over the 100 simulations of a best-fitting IMF (first row) and a Kroupa IMF (second row) with corresponding p -values. D_{\min} and p_{\min} are also given for the single best-fitting MSLF from each set of simulations.

(M_U, α)	D_{ave}	p_{ave}	D_{\min}	p_{\min}
$(16 M_{\odot}, -2.45)$	0.108	0.288	0.065	0.884
$(120 M_{\odot}, -2.35)$	0.136	0.088	0.096	0.438

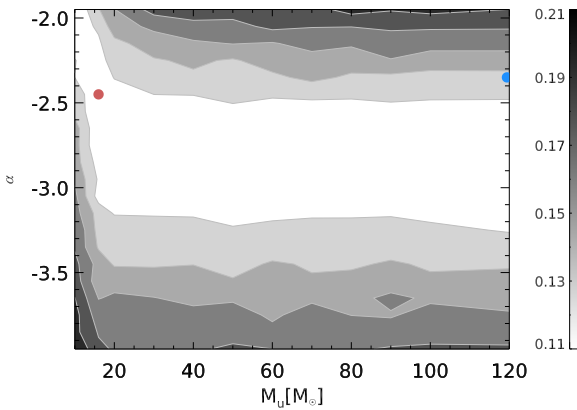


Figure 6. Contour plot of mean KS test D statistic across the (M_U, α) parameter space. The red point corresponds to the best-fitting IMF parameters, and the blue point to a Kroupa IMF.

In §3.1 we provided justification for our assumption of a constant SFH, but have not provided any sanity checks to confirm that this assumption is correct. The population of BL stars can be used to provide such a check. Our first sanity check compares the cumulative luminosity function of observed BL stars to simulation populations. Like the MSLF analysis, the Kroupa IMF simulations over-predict the number of BL stars compared to the observations. The best-fit IMF simulations are a closer match the BL luminosity function, but slightly under-predict the number of bright BL stars. Our second sanity check compares the ratio of BL to MS stars to the observed fraction $\text{BL/MS} = 0.660$. The average BL/MS ratio of the 100 simulations assuming a best-fit and Kroupa IMF are 0.644 ± 0.017 and 0.571 ± 0.015 respectively, where the uncertainties are the standard deviations. Clearly, best-fit IMF better reproduces the observed MS and BL stars under the assumption of a constant SFH.

4.2 Uncertainties in IMF parameters

We ran simulations to determine how well our method recovers an IMF of known input and the uncertainty on the derived parameters. We generated mock observations by randomly selecting stars equal in number to the observed MS (162) from the 100 Kroupa and best-fitting IMF simulations. The KS test comparison is then rerun for each mock population against the entire grid of models to determine the best-fitting IMF parameters, and we use the mean and standard deviation of the distribution of recovered param-

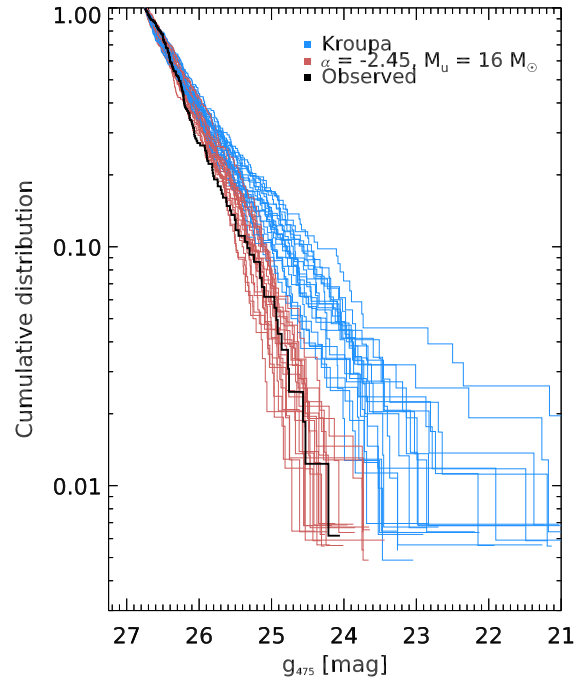


Figure 7. Comparison of cumulative MSLFs between that observed in DDO 154 (black) and the 20 best-fitting simulations from a Kroupa IMF (blue) and best-fitting IMF (red).

eters to quantify the uncertainties. For an input Kroupa IMF the average recovered parameters are $\alpha = -2.31 \pm 0.29$ and $M_U = 61 \pm 35 M_{\odot}$, and for an input best-fitting IMF $\alpha = -2.58 \pm 0.37$ and $M_U = 36 \pm 29 M_{\odot}$. However, only the distribution of recovered α values for the best-fitting IMF are Gaussian; the uncertainty in M_U is more lopsided as shown in Fig. 8. The large uncertainties quoted are consistent with the width and length of the region of local minima observed in Fig. 6.

4.3 Caveats

Here we consider the assumptions we have made when modelling CMDs, and the effects they could have on our results.

The evolutionary tracks we use do not include the effects of stellar rotation, which causes stars to have longer MS lifetimes, higher effective temperatures, rates of mass loss (Ekström et al. 2012), and by the MS turnoff, a higher luminosity (Potter et al. 2012). If our simulated stars turn off the MS early compared to the observed population, then there will appear to be an over-abundance of high mass stars, requiring IMF parameters that are flatter or have a higher upper mass limit to match the observations. This is also the case for the luminosity of the stars, if the non-rotating stars are fainter, then our simulations would require more high mass stars to match the observations, biasing us toward flatter IMF slopes and higher upper mass limits.

We do not model the effects of binary stellar evolution (Eldridge et al. 2017), nor the presence of binary systems or star clusters. Typical binary separations are ~ 10 AU (Minor 2013) which are unresolved at the pixel scale 0.974 pc/pix of the images; effectively all binaries are unresolved in our

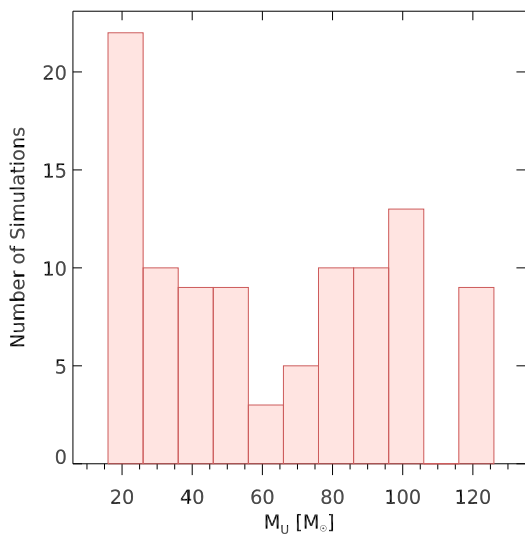


Figure 8. Histogram of the 100 recovered M_U values from KS tests of mock observations created from the best-fit IMF simulations.

data. Similarly, there could be unresolved low mass clusters in the images appearing as bright stars. Hill & Zaritsky (2006) find the average core radius of LMC clusters to be 4.2 pc which would be resolved by our images, but some of their more compact observed clusters have core radii of just 0.61 pc which would be unresolved. Weidner et al. (2009) investigated the effects of unresolved stellar multiplicity up to order four on determinations of the IMF. They found that even in the most extreme cases (100% stellar multiplicity) the effect on the observed IMF is small, within the uncertainties of most studies. It is only below system masses of $0.5 M_{\odot}$ that binaries begin to effect the observed luminosity function significantly (Kroupa et al. 1991, 1993), hence the effects of unresolved multiplicity on our results should not be significant. However, to the extent that unresolved stellar multiplicity is present, it would cause us to overestimate the number of high mass stars and bias our results toward a higher M_U or flatter α than the true IMF.

Interacting binaries may also complicate the interpretation of these results (Eldridge & Stanway 2009; Yang et al. 2011; Li et al. 2012, e.g.). They have been typically been ignored in other studies of resolved stellar populations (e.g. Aparicio & Gallart 2004; Weisz et al. 2011; Lewis et al. 2015); as their effects on the observed CMD are dependant on many parameters such as mass transfer and initial binary distribution (Larsen et al. 2011; Eldridge et al. 2017).

We model a uniform reddening across the field of view equal to the foreground $E(B - V)^G = 0.009$ (Jacobs et al. 2009) and neglect the effects of internal dust extinction. Although such an approach is common in the literature (e.g. McConnell et al. 2005; Williams et al. 2009b; Hillis et al. 2016) it raises concerns since young stars should be found close to their birth clouds, where the ISM is still dense and clumpy, and young star clusters are likely to have higher levels of internal extinction than old ones (Grosbøl & Dottori 2012). This would add intrinsic scatter to the CMD which

we have not modelled. We examined the $V - I$ versus $g - V$ two colour diagram and find no detectable net reddening of MS stars to the limit of $E(B - V) \lesssim 0.1$, which is too loose of a constraint to be useful in this study. We justify our approach by noting that a low amount of internal dust is expected for the outer disc of DDO 154 since it is far removed from the star-forming centre. Furthermore, the dust content in galaxies has been observed to decrease with galactocentric radius (Muñoz-Mateos et al. 2009), the dust to gas mass ratio is lower in low metallicity systems (Rémy-Ruyer et al. 2014) such as DDO 154 ($Z = 0.1Z_{\odot}$, see Table. 1). Many dwarf galaxies have little or no detectable dust (van Zee 2000); the SINGS (Kennicutt et al. 2003) and KINGFISH (Kennicutt et al. 2011; Rémy-Ruyer et al. 2014) surveys detect no far infrared dust emission from DDO 154 using *Spitzer* and *Herschel* data. Hence scatter on the CMD due to internal extinction should not be significant.

Overall, neglecting stellar rotation and multiplicity would bias us toward overestimating the number of high mass stars, or equivalently deriving a flatter α or higher M_U than the true IMF. As the best-fitting IMF is already steeper and deficient in high mass stars compared to a universal Kroupa IMF, the true deficiency of high mass stars is likely underestimated by our results.

5 STAR FORMATION IN THE OUTER DISC

5.1 Local star formation law

Figure 9 shows the correlation between the MS stars and the H I surface density (Σ_{HI}) from the THINGS survey (Walter et al. 2008). We used the natural weighted map (resolution $6'' = 117$ pc) for better sensitivity to diffuse emission. The MS stars are mostly located in the bottom half of our images, as displayed in Figures 4 and 9, closest to the optically bright central region of the galaxy (beyond the edge of our images) and where Σ_{HI} is the highest within our frame (Fig. 5). There are very few MS stars beyond $R \approx 6$ kpc where $\Sigma_{\text{HI}} \leq 2 M_{\odot} \text{pc}^{-2}$. Even the BL stars which trace the formation of stars with masses down to $\sim 2.6 M_{\odot}$, and hence ages up to ~ 420 Myr ago, appear to be scarce in the outer disc. The red bar in Fig. 9 corresponds to the maximum distance a $4 M_{\odot}$ star could travel over its MS lifetime travelling at the typical H I velocity dispersion in our *HST* images of 8.62 km s^{-1} . The two farthest MS stars fall within this tolerance of ASN-1 (marked by a red circle). Hence it is unclear whether these stars were formed in situ at high radii, or have drifted from a different formation site. The relative quiescence of the outer disc is an interesting contrast to the studies of Gil de Paz et al. (2005) and Thilker et al. (2005, 2007) who find that UV bright star formation is common in extended outer discs.

To parameterise the SFL we compare Σ_{HI} to the SFR surface density (Σ_{SFR}) derived from the surface density of MS stars (Σ_{MS}). We count the number of MS stars in bins of 0.1 dex in Σ_{HI} and divide by the inclination corrected pixel area covered by each bin, equivalent to the method used by Sanduleak (1969) and B15. Σ_{MS} is then converted to Σ_{SFR} assuming a Kroupa (or best-fit) IMF slope for $m \geq 1 M_{\odot}$, and the Kroupa (2001) broken power law for $0.08 M_{\odot} \leq m < 1 M_{\odot}$. The conversion factors for a Kroupa IMF and a best-fit IMF are 2.2 and $2.36 (\times 10^{-6}) M_{\odot} \text{ yr}^{-1} \text{ star}^{-1}$ respectively.

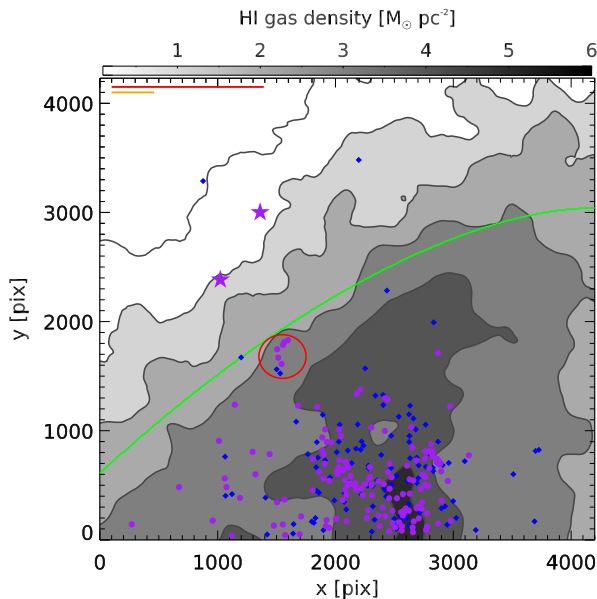


Figure 9. The spatial correlation between MS (purple) and BL (blue diamonds) stars and the surface density of HI in the *HST*/ACS field of view. HI contours are at 0.5, 1, 2, 4 and 6 $M_{\odot} \text{pc}^{-2}$. The red and orange bars in the top left corner denote the distances stars in our selection box could travel over the MS lifetime of a 4 M_{\odot} and 26 M_{\odot} star respectively if travelling at the HI velocity dispersion. The green contour corresponds to a radius of 6 kpc in the disc plane.

Fig. 10 compares our derived SFL to the standard K-S SFL (Kennicutt 1998) and the SFL derived for dwarf galaxies by Bigiel et al. (2010). Here we adopt a Kroupa IMF to be consistent with these and other previous studies. A linear, error-weighted least squares fit to our data gives a SFL with slope $N = 2.92 \pm 0.22$ and zero point $A = 4.47 \pm 0.65 \times 10^{-7} M_{\odot} \text{yr}^{-1} \text{kpc}^{-2}$. If we assume our best-fitting IMF the zero point becomes $A = 4.82 \pm 0.71 \times 10^{-7} M_{\odot} \text{yr}^{-1} \text{kpc}^{-2}$. Star formation appears to become quickly suppressed as $\log_{10}(\Sigma_{\text{HI}}/M_{\odot} \text{pc}^{-2})$ falls below ~ 0.7 . Our derived power-law slope is typical of the values determined for dwarf irregular galaxies by Roychowdhury et al. (2009, at 200 pc and 400pc spatial resolution, compared to our 117pc), but there are some differences. The total HI mass of DDO 154 is an order of magnitude higher when compared to galaxies with a similar N value, which shows up as a difference in the value of the zero point. Galaxies from Roychowdhury et al. (2009) such as UGC 8215 ($N = 3.1$, $A = 1.99 \times 10^{-6} M_{\odot} \text{yr}^{-1} \text{kpc}^{-2}$) and DDO 181 ($N = 2.6$, $A = 1.48 \times 10^{-5} M_{\odot} \text{yr}^{-1} \text{kpc}^{-2}$) both have similar N values to DDO 154, but much higher A values. It is only when we compare just the HI mass in our *HST* field of view ($6.1 \times 10^7 M_{\odot}$) to the total HI mass of these galaxies, that the N values and HI masses show a correspondence.

The Bigiel et al. (2010) data differs from ours as they derive SFR from UV surface brightness and average Σ_{HI} over 750 pc boxes whereas our SFL is calculated by counting stars within HI isophotes. Nevertheless, the majority of our data points are within the scatter of the Bigiel et al. (2010) measurements. Interestingly, Fig. 10 shows measuring Σ_{SFR} leads to values significantly lower than those obtained

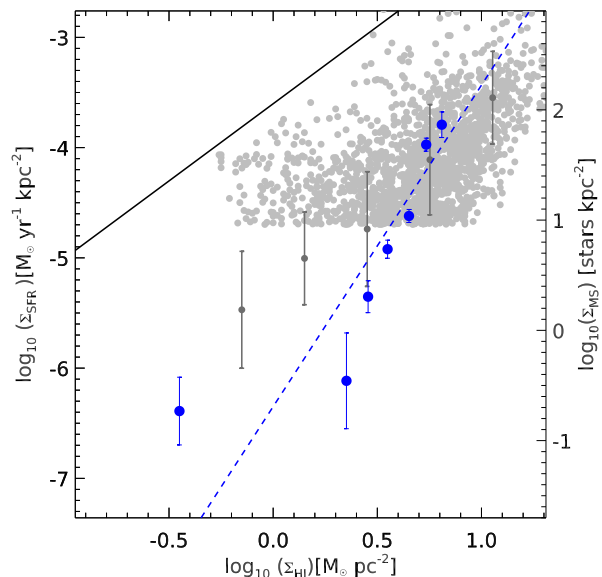


Figure 10. The local SFL in the outer disc of DDO 154 derived from the surface density of MS stars assuming a Kroupa IMF shown as blue points with error bars. The blue dashed line represents our linear, error weighted, least squares fit to the data and the black line shows the Kennicutt (1998) SFL with $N = 1.4$ for the bright part of galaxies. The SFL for dwarf galaxies from Bigiel et al. (2010) is shown as grey points with median values given in darker grey with error bars.

from GALEX. This is also suggested by Fig. 5 where some MS stars do not have correlated NUV emission. When compared to the SFL derived in the outskirts of massive galaxies from the The Local Volume HI Survey (LVHIS, Wang et al. 2017), their Σ_{SFR} values sit mostly above the median trend of Bigiel et al. (2010), whereas ours is consistently below it, reflecting the dormancy of the outer disc of DDO 154. It is commonly observed that the central regions of dwarf galaxies have a similar SFL to outer discs of spirals (e.g. Bigiel et al. 2010; Roychowdhury et al. 2015). Our method assumes that the gas and stars have not moved since the birth of the stars. In reality stars may have migrated causing a potential underestimation of Σ_{SFR} in regions of higher Σ_{HI} , and an overestimation where Σ_{HI} is lower. Potentially biasing N to be flatter than the true SFL.

5.2 Comparison to theory

Krumholz (2013) suggests that differences in the SFL observed between the bright centres of galaxies, and outer discs and dwarf galaxies is due to the processes that govern the conversion of HI to H_2 . He modelled star formation in HI dominated conditions and found results consistent with the observations of Bigiel et al. (2010). In Fig. 11 we compare our observed SFL to models of star formation in HI dominated regions by Ostriker et al. (2010) and Krumholz (2013). The key parameter in both models is the combined volume density of stars and dark matter, ρ_{sd} , and the gas metallicity in the case of Krumholz (2013). Our data favours the Krumholz (2013) models but is steeper than both, favouring $\rho_{\text{sd}} = 0.1 M_{\odot} \text{pc}^{-3}$ at higher $\log_{10}(\Sigma_{\text{HI}})$

and $\rho_{\text{sd}} = 0.01 M_{\odot} \text{pc}^{-3}$ at lower. Overall the data appears to favour the lower density model, so we assume this density to be the best-fit to the data.

How does this compare to the stellar densities predicted by the IMF analysis? The expected density of stars depends on the timescale that star formation has persisted. We take the minimum star formation timescale to be the minimum orbital time in the *HST* images (~ 743 Myr, at a radius 2.3 kpc) and the maximum being the Hubble time. The volume density of stars depends on the scale height of the disc, for which we choose a typical value of $h \sim 100$ pc. Assuming a Kroupa IMF the face on SFR surface density in our optical images is $3.99 \times 10^{-6} M_{\odot} \text{yr}^{-1} \text{kpc}^{-2}$, corresponding to minimum and maximum stellar volume densities for a disc of thickness $2h$ of $\rho_{\text{s,min}} = 1.48 \times 10^{-5} M_{\odot} \text{pc}^{-3}$ and $\rho_{\text{s,max}} = 2.73 \times 10^{-4} M_{\odot} \text{pc}^{-3}$. If our best-fitting IMF is used instead, these values are 1.08 times larger. These stellar density estimates are too low to account our SFL results which best match the Krumholz (2013) $\rho_{\text{sd}} = 0.01 M_{\odot} \text{pc}^{-3}$ theoretical model. Mass modelling of DDO 154 by Carignan & Purton (1998) also predicts the density of dark matter alone would also be too low: $\rho_{\text{d}} = 0.015 M_{\odot} \text{pc}^{-3}$ at 1.4 kpc and $\rho_{\text{d}} = 0.001 M_{\odot} \text{pc}^{-3}$ at 6.1 kpc. We determine the maximum allowable mass density using the THINGS rotation curve (Walter et al. 2008) to find the mass enclosed in the radii range covered by our *HST* images (2.3 kpc — 12.2 kpc). Assuming a uniform density ring of thickness $2h$ we find $\rho_{\text{max}} = 0.061 M_{\odot} \text{pc}^{-3}$, which is higher than the Krumholz (2013) $\rho_{\text{sd}} = 0.01 M_{\odot} \text{pc}^{-3}$ model. Hence, these models work best if the dark matter is somewhere in-between a spherical distribution, and a flattened disc like system. This could imply energy dissipation contrary to the standard CDM scenario (e.g. Davis et al. 1985; Peebles 2017), or as we only consider the two extreme scenarios there could be geometric factors which we are not accounting for.

5.3 Total star formation rate

We determine the SFR integrated over the disc of DDO 154 to be $3.14 \times 10^{-3} M_{\odot} \text{yr}^{-1}$ assuming our derived SFL applies for the entire gas disc with an adopted Kroupa IMF. This is within the uncertainties of the $\text{H}\alpha$ based SFR estimates, and slightly lower than the UV+IR SFR from the literature (see Table 1). Adopting our best-fitting IMF increases the SFR by a factor of 1.08 slightly improving the comparison to previous estimates of the UV+IR SFR. However, these published values cover just the central region of the galaxy which is largely outside our field of view and where star formation would be expected to be more ‘normal’. If we restrict the integrated SFR to radii greater than the $R_{25} = 3.61$ kpc (de Vaucouleurs et al. 1991) we find the SFR of the outer disc to be $1.20 \times 10^{-3} M_{\odot} \text{yr}^{-1}$ assuming a Kroupa IMF. This is 24% of the UV+IR SFR estimate of the central region of the galaxy, a significant but not dominant contribution to the total SFR of the galaxy. This corresponds to a face on SFR surface density for $R > R_{25}$ of $2.80 \times 10^{-6} M_{\odot} \text{yr}^{-1} \text{kpc}^{-2}$, which is typical of the intensities observed in the outer discs of spirals (10^{-6} — $10^{-5} M_{\odot} \text{yr}^{-1} \text{kpc}^{-2}$, Barnes et al. 2012) and other dwarf galaxies (e.g. NGC 2915: $1.8 \times 10^{-5} M_{\odot} \text{yr}^{-1} \text{kpc}^{-2}$, B15).

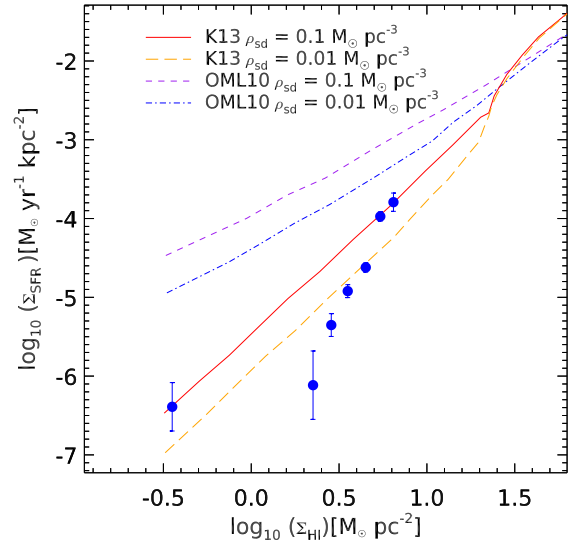


Figure 11. Comparison of the SFL in the outer disc of DDO 154 (the same as Fig. 10) to the theoretical models of Ostriker et al. (2010, OML10) and Krumholz (2013, K13). We show models for the combined volume density of stars and dark matter $\rho_{\text{sd}} = 0.1 M_{\odot} \text{pc}^{-3}$ and $\rho_{\text{sd}} = 0.01 M_{\odot} \text{pc}^{-3}$ for our adopted metallicity $Z = 0.1 Z_{\odot}$.

5.4 IGIMF theory

So far, we have modelled star formation purely stochastically: without clustering in space or time. However, the formation of stars appears to be highly correlated, with new stars tending to form in embedded clusters, associations, or groups many of which later dissolve (Lada & Lada 2003). One approach to account for this is to use the Integrated Galaxy-wide Initial Mass Function (IGIMF) framework (Weidner & Kroupa 2005, 2006; Weidner et al. 2010; Yan et al. 2017), whereby all stars are born in clusters adhering to a well behaved IMF with an upper mass limit that varies but is set by the cluster mass, a SFR-dependant single-slope power law cluster mass function (Yan et al. 2017), and a maximum cluster mass set by the SFR. When integrated over all the star-forming clusters in a galaxy that is weakly forming stars the IGIMF is top light compared to the universal IMF (it is top heavy at high star formation rates). In Fig. 12 we compare the best-fit IMF we derive for the outskirts of DDO154 ($M_U = 16 M_{\odot}$, $\alpha = -2.45$), with the distribution of stellar masses we expect from IGIMF theory following Yan et al. (2017). We use our adopted metallicity ($Z = 0.1 Z_{\odot}$) and a SFR of $4.65 \times 10^{-4} M_{\odot} \text{yr}^{-1}$, the total SFR in our *HST*/ACS field of view assuming a best-fit IMF. For comparison we also display a standard Kroupa (Kroupa 2001) IMF (with an offset so as not to clutter the figure). We see that our best-fit IMF is very similar to that predicted by IGIMF theory. The low SFR of DDO154 is thus similar to the low density outskirts of the Orion nebula which appear deficient in O and B stars (Megeath et al. 2016).

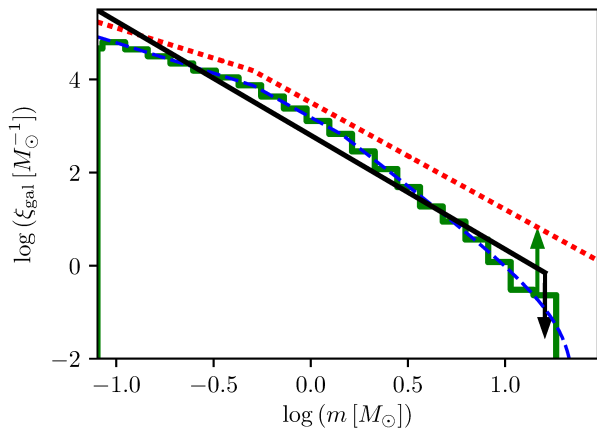


Figure 12. Comparison between the best-fit IMF (black), Kroupa IMF (red, offset +0.5 dex), prediction from IGIMF theory (blue, dashed), and the optimally sampled galaxy-wide IMF (green). The upper mass limit from the best-fit IMF $M_U = 16 M_\odot$ is shown by a black downward pointing arrow, and the optimally sampled prediction $m = 15 M_\odot$ by a green upward arrow.

5.5 Stability of the outer disc

Insight into the dynamics of the dormant and star-forming parts of the outer disc can be provided by the HI data. Using the THINGS rotation curve (Walter et al. 2008) and adopting a flat velocity dispersion of $\sigma_g = 8.62 \text{ km s}^{-1}$ we create a spatial map of the Toomre Q parameter of the HI in our optical images. We transform and re-grid the maps to the field of view and resolution of our optical images, and calculate radii in the disc plane assuming the tilted ring model of de Blok et al. (2008). The Toomre (1964) Q parameter is given by

$$Q = \frac{\sigma_g \kappa}{\pi G \Sigma_{\text{gas}}}, \quad (1)$$

where σ_g is the gas velocity dispersion, G is the gravity constant, and κ is the epicyclic frequency given by

$$\kappa = 1.41 \frac{V_c(R)}{R} \sqrt{1 + \frac{d \log V_c(R)}{d \log R}}. \quad (2)$$

Adopting $\Sigma_{\text{gas}} = \Sigma_{\text{HI}}$, Fig. 13 shows the distribution of the Q parameter in our *HST* images. Almost all of the MS and BL stars appear to be in regions where $Q \leq 4$. We compare histograms of HI mass and star counts as a function of Q in Fig. 14. There is a strong peak in HI mass and star counts at $Q \approx 2$ to 3, and a clearly extended tail of high Q gas corresponding to the extended outer disc (the dark regions in Fig. 13). Quantitatively, 28% of the HI mass in our *HST*/*ACS* images has stability parameter $Q \geq 4$ while only 2.5% of the MS stars and 9.3% of the BL stars exist in regions with this stability and higher. In Fig. 15 we compare radially averaged profiles of Q , κ and Σ_{HI} . The rise in Q beyond $R \approx 6$ kpc can be seen to be driven by the rapid decrease in Σ_{HI} which is proceeding faster than the decrease in κ . This is consistent with Meurer et al. (2013), who observe Q transition from flat to rising at high radii in disc galaxies.

The high stability of the outer disc may be causing the absence of young stars. Star formation traced by $\text{H}\alpha$ emission is typically truncated when the stability parameter Q exceeds a threshold, corresponding to $Q \approx 2.1$

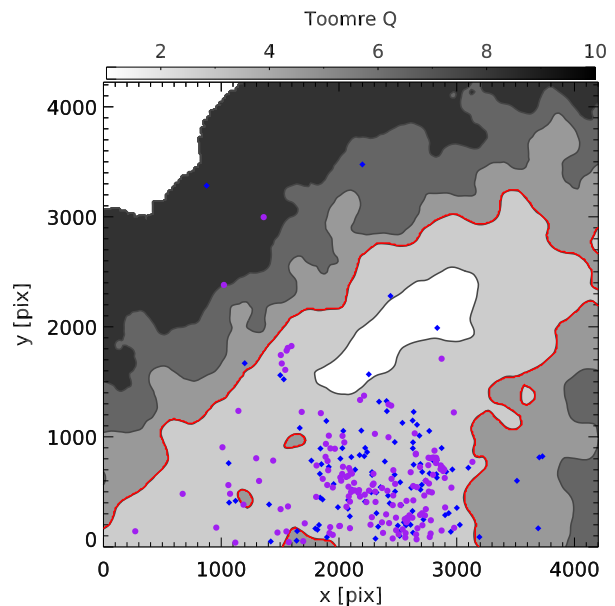


Figure 13. Contour plot of the Toomre Q parameter across the *HST*/*ACS* field of view with MS (purple) and BL (blue diamonds) shown for spatial comparison. The contours are spaced at $Q = 2, 4, 6,$ and 10 with the scale given by the colour bar at the top. The red contour corresponds to $Q = 4$, and the white region in the top left is where the data ends.

(Kennicutt 1989; Martin & Kennicutt 2001). This coincides with the peak Q of the young stars in Fig. 14 implying that star formation is truncated where the disc is stable; hence our results are consistent with Kennicutt (1998) and Martin & Kennicutt (2001). However, this result is in contrast to the discovery that outer discs often exhibit UV bright star formation even where $\text{H}\alpha$ emission is weak or absent (Gil de Paz et al. 2005; Thilker et al. 2005, 2007). The outer disc of DDO154 is nearly dormant according to all available star formation tracers, but may contain star formation below our detection limit.

6 CONCLUSIONS

Stellar populations uniquely determine the vast majority of the observed properties of galaxies such as metallicity, surface brightness, and emission line strengths. While the stellar initial mass function (IMF) is commonly assumed to be invariant regardless of the star-forming environment, there is strong evidence of real variations of the properties of its upper mass end (Hoversten & Glazebrook 2008; Meurer et al. 2009; Lee et al. 2009; Dabringhausen et al. 2010; Gunawardhana et al. 2011; Marks et al. 2012; Romano et al. 2017; Schneider et al. 2018). We have placed constraints on the high mass slope of the IMF using the Main Sequence Luminosity Function extracted from an optical colour magnitude diagram (CMD) of the resolved population of stars in the extended HI outer disc of the dwarf irregular galaxy DDO 154.

Our main results are as follows: The IMF required to match the observed population of main sequence (MS) stars is deficient in high mass stars compared to a standard Kroupa IMF (Kroupa 2001). The Kroupa IMF is ruled out

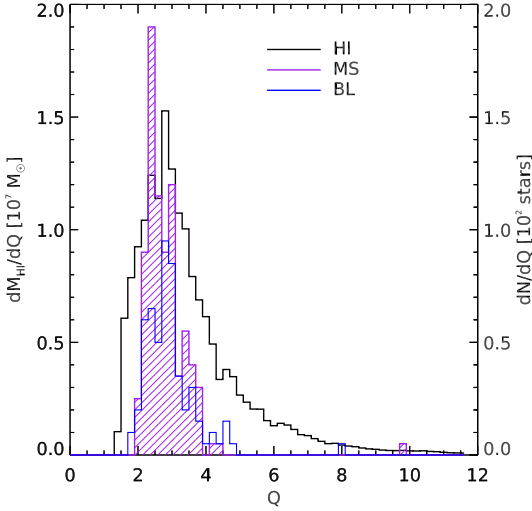


Figure 14. Histogram comparing the distribution of HI mass (black, left axis) in the *HST* field of view and the number of MS (purple, shaded) and BL (blue) stars (right axis) as a function of the Q parameter.

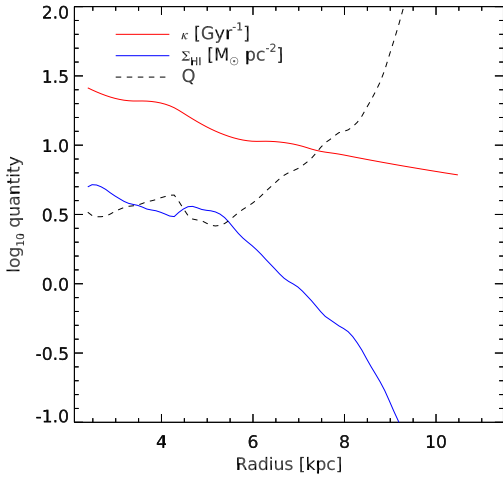


Figure 15. Radially averaged profiles of κ , Q and Σ_{HI} in the *HST* field of view. The rapid increase in Q beyond $R = 6$ kpc coincides with steeper decline in Σ_{HI} , while κ falls steadily.

to a $p = 0.088$ significance level using a KS test between the observed MS stars and our simulated stellar populations. We find that the star formation rate (SFR) in the outer disc is consistent with observations of other dwarf galaxies, where star formation is suppressed below the standard Kennicutt-Schmidt law observed in the bright portions of galaxies (Kennicutt 1989, 1998; Martin & Kennicutt 2001; Bigiel et al. 2008). Our best-fit IMF agrees with the predictions of IGIMF theory, thus star formation in this outer disc is similar to the low density regions of the Orion nebula (Megeath et al. 2016). Deeper observations of extended discs would provide insight to whether low mass stars are forming, as these observations point to an IMF deficient in the highest mass stars.

A stand out feature of previous studies is that star formation in the outer discs of galaxies is common (e.g. Gil de Paz et al. 2005; Thilker et al. 2005, 2007) and appears to follow the HI (Cuillandre et al. 2001; Pflamm-Altenburg & Kroupa 2008; B15). In this work, we find star formation is absent in much of outer disc of DDO 154, at least in terms of stars of mass $m > 4 M_{\odot}$. The high stability parameter $Q > 4$ of the extended HI disc demonstrates that some galaxies can maintain a large reservoir of ISM which is dormant in high mass star formation. It is not known how common these dormant discs are.

ACKNOWLEDGEMENTS

We thank the anonymous referee for their helpful comments that improved this paper. AW, GRM, KP and TJ acknowledge financial support through the DAAD (The Australian - Germany Joint Research Co-operation Scheme) throughout the course of this work. PK and TJ thank the DAAD for supporting this project with travel grant 57212729, "Galaxy formation with a variable stellar initial mass function". TJ was supported by the University of Bonn and by Charles University through the grant SVV-260441.

This project was initiated as part of the Advanced Camera for Surveys (ACS) Instrument Definition Team effort. ACS was developed under NASA contract NAS 5-32865, and this research has been supported by NASA grant NAG5-7697 and by an equipment grant from Sun Microsystems, Inc. Some/all of the HST and POSS data presented in this paper were obtained from the Mikulski Archive for Space Telescopes (MAST). STScI is operated by the Association of Universities for Research in Astronomy, Inc., under NASA contract NAS5-26555. Support for MAST for non-HST data is provided by the NASA Office of Space Science via grant NNX09AF08G and by other grants and contracts.

REFERENCES

- Annibali F., et al., 2013, *AJ*, 146, 144
 Aparicio A., Gallart C., 2004, *AJ*, 128, 1465
 Asplund M., Grevesse N., Sauval A. J., Scott P., 2009, *ARA&A*, 47, 481
 Baldry I. K., Glazebrook K., Driver S. P., 2008, *MNRAS*, 388, 945
 Barker M. K., Sarajedini A., Geisler D., Harding P., Schommer R., 2007, *AJ*, 133, 1138
 Barnes K. L., van Zee L., Côté S., Schade D., 2012, *ApJ*, 757, 64
 Barris B. J., Tonry J. L., 2006, *ApJ*, 637, 427
 Bastian N., Covey K. R., Meyer M. R., 2010, *ARA&A*, 48, 339
 Bate M. R., Bonnell I. A., 2005, *MNRAS*, 356, 1201
 Bate M. R., Bonnell I. A., Bromm V., 2003, *MNRAS*, 339, 577
 Bertelli Motta C., Clark P. C., Glover S. C. O., Klessen R. S., Pasquali A., 2016, *MNRAS*, 462, 4171
 Bigiel F., Leroy A., Walter F., Brinks E., de Blok W. J. G., Madore B., Thornley M. D., 2008, *AJ*, 136, 2846
 Bigiel F., Leroy A., Walter F., Blitz L., Brinks E., de Blok W. J. G., Madore B., 2010, *AJ*, 140, 1194
 Bonnell I. A., 2008, in Knapen J. H., Mahoney T. J., Vazdekis A., eds, *Astronomical Society of the Pacific Conference Series* Vol. 390, *Pathways Through an Eclectic Universe*. p. 26
 Bonnell I. A., Bate M. R., 2002, *MNRAS*, 336, 659
 Bressan A., Marigo P., Girardi L., Salasnich B., Dal Cero C., Rubele S., Nanni A., 2012, *MNRAS*, 427, 127
 Bressert E., et al., 2010, *MNRAS*, 409, L54

- Bruzzese S. M., Meurer G. R., Lagos C. D. P., Elson E. C., Werk J. K., Blakeslee J. P., Ford H., 2015, *MNRAS*, 447, p. 618 (B15)
- Cappellari M., et al., 2012, *Nature*, 484, 485
- Carignan C., Freeman K. C., 1988, *ApJL*, 332, L33
- Carignan C., Purton C., 1998, *ApJ*, 506, 125
- Castelli F., Kurucz R. L., 2004, arXiv e-prints (astro-ph/0405087)
- Chabrier G., 2003, *PASP*, 115, 763
- Cignoni M., Cole A. A., Tosi M., Gallagher J. S., Sabbi E., Anderson J., Grebel E. K., Nota A., 2012, *ApJ*, 754, 130
- Conroy C., van Dokkum P. G., 2012, *ApJ*, 760, 71
- Cuillandre J.-C., Lequeux J., Allen R. J., Mellier Y., Bertin E., 2001, *ApJ*, 554, 190
- Dabringhausen J., Fellhauer M., Kroupa P., 2010, *MNRAS*, 403, 1054
- Dalcanton J. J., et al., 2009, *ApJS*, 183, 67
- Dalcanton J. J., et al., 2012, *ApJS*, 200, 18
- Davis T. A., McDermid R. M., 2017, *MNRAS*, 464, 453
- Davis M., Efstathiou G., Frenk C. S., White S. D. M., 1985, *ApJ*, 292, 371
- Dessauges-Zavadsky M., Verdugo C., Combes F., Pfenniger D., 2014, *A&A*, 566, A147
- Dolphin A. E., 2000, *PASP*, 112, 1383
- Dolphin A. E., 2002, *MNRAS*, 332, 91
- Dopita M. A., Ryder S. D., 1994, *ApJ*, 430, 163
- Ekström S., et al., 2012, *A&A*, 537, A146
- Eldridge J. J., Stanway E. R., 2009, *MNRAS*, 400, 1019
- Eldridge J. J., Stanway E. R., Xiao L., McClelland L. A. S., Taylor G., Ng M., Greis S. M. L., Bray J. C., 2017, *PASA*, 34, e058
- Elmegreen B. G., 1999, *ApJ*, 515, 323
- Elmegreen B. G., 2004, *MNRAS*, 354, 367
- Elmegreen B. G., 2008, *ApJ*, 672, 1006
- Ferguson H. C., Babul A., 1998, *MNRAS*, 296, 585
- Freedman W. L., 1985, *ApJ*, 299, 74
- Geha M. C., et al., 1998, *AJ*, 115, 1045
- Geha M., et al., 2013, *ApJ*, 771, 29
- Gennaro M., et al., 2018, *ApJ*, 855, 20
- Gerola H., Seiden P. E., Schulman L. S., 1980, *ApJ*, 242, 517
- Gieles M., Moeckel N., Clarke C. J., 2012, *MNRAS*, 426, L11
- Gil de Paz A., et al., 2005, *ApJL*, 627, L29
- Grosbøl P., Dottori H., 2012, *A&A*, 542, A39
- Gunawardhana M. L. P., et al., 2011, *MNRAS*, 415, 1647
- Gutermuth R. A., Pipher J. L., Megeath S. T., Myers P. C., Allen L. E., Allen T. S., 2011, *ApJ*, 739, 84
- Harris J., Zaritsky D., 2004, *AJ*, 127, 1531
- Harris J., Zaritsky D., 2009, *AJ*, 138, 1243
- Harris J., Calzetti D., Gallagher III J. S., Smith D. A., Conselice C. J., 2004, *ApJ*, 603, 503
- Hill A., Zaritsky D., 2006, *AJ*, 131, 414
- Hillis T. J., Williams B. F., Dolphin A. E., Dalcanton J. J., Skillman E. D., 2016, *ApJ*, 831, 191
- Hoversten E. A., Glazebrook K., 2008, *ApJ*, 675, 163
- Jacobs B. A., Rizzi L., Tully R. B., Shaya E. J., Makarov D. I., Makarova L., 2009, *AJ*, 138, 332
- Kalari V. M., 2017, in *Revista Mexicana de Astronomía y Astrofísica Conference Series*. pp 89–89
- Kalirai J. S., et al., 2013, *ApJ*, 763, 110
- Karachentsev I. D., Karachentseva V. E., Huchtmeier W. K., Makarov D. I., 2004, *AJ*, 127, 2031
- Karachentsev I. D., Makarov D. I., Kaisina E. I., 2013, *AJ*, 145, 101
- Kennicutt Jr. R. C., 1989, *ApJ*, 344, 685
- Kennicutt Jr. R. C., 1998, *ApJ*, 498, 541
- Kennicutt Jr. R. C., Skillman E. D., 2001, *AJ*, 121, 1461
- Kennicutt Jr. R. C., et al., 2003, *PASP*, 115, 928
- Kennicutt R. C., et al., 2011, *PASP*, 123, 1347
- Koda J., Yagi M., Boissier S., Gil de Paz A., Imanishi M., Donovan Meyer J., Madore B. F., Thilker D. A., 2012, *ApJ*, 749, 20
- Kroupa P., 2001, *MNRAS*, 322, p. 231
- Kroupa P., Gilmore G., Tout C. A., 1991, *MNRAS*, 251, 293
- Kroupa P., Tout C. A., Gilmore G., 1993, *MNRAS*, 262, 545
- Kruijssen J. M. D., 2012, *MNRAS*, 426, 3008
- Krumholz M. R., 2011, *ApJ*, 743, 110
- Krumholz M. R., 2013, *MNRAS*, 436, 2747
- Krumholz M. R., 2014, *Phys. Rep.*, 539, 49
- Krumholz M. R., Klein R. I., McKee C. F., 2012, *ApJ*, 754, 71
- La Barbera F., Ferreras I., Vazdekis A., 2015, *MNRAS*, 449, L137
- Lada C. J., Lada E. A., 2003, *ARA&A*, 41, 57
- Larsen S. S., Richtler T., 2000, *A&A*, 354, 836
- Larsen S. S., et al., 2011, *A&A*, 532, A147
- Lee H.-c., Gibson B. K., Flynn C., Kawata D., Beasley M. A., 2004, *MNRAS*, 353, 113
- Lee J. C., et al., 2009, *ApJ*, 706, 599
- Leroy A. K., Walter F., Brinks E., Bigiel F., de Blok W. J. G., Madore B., Thornley M. D., 2008, *AJ*, 136, 2782
- Leroy A. K., et al., 2013, *AJ*, 146, 19
- Lewis A. R., et al., 2015, *ApJ*, 805, 183
- Li Z., Mao C., Chen L., Zhang Q., 2012, *ApJL*, 761, L22
- Mannucci F., Maoz D., Sharon K., Botticella M. T., Della Valle M., Gal-Yam A., Panagia N., 2008, *MNRAS*, 383, 1121
- Marks M., Kroupa P., Dabringhausen J., Pawlowski M. S., 2012, *MNRAS*, 422, 2246
- Martin C. L., Kennicutt Jr. R. C., 2001, *ApJ*, 555, 301
- Martín-Navarro I., et al., 2015, *ApJL*, 798, L4
- McConnachie A. W., Irwin M. J., Ferguson A. M. N., Ibata R. A., Lewis G. F., Tanvir N., 2005, *MNRAS*, 356, 979
- McQuinn K. B. W., et al., 2010a, *ApJ*, 721, 297
- McQuinn K. B. W., et al., 2010b, *ApJ*, 724, 49
- McQuinn K. B. W., Skillman E. D., Dalcanton J. J., Cannon J. M., Dolphin A. E., Holtzman J., Weisz D. R., Williams B. F., 2012, *ApJ*, 759, 77
- Megeath S. T., et al., 2016, *AJ*, 151, 5
- Meurer G. R., 2000, in Lançon A., Boily C. M., eds, *Astronomical Society of the Pacific Conference Series Vol. 211, Massive Stellar Clusters*. p. 81
- Meurer G. R., Heckman T. M., Leitherer C., Kinney A., Robert C., Garnett D. R., 1995, *AJ*, 110, 2665
- Meurer G. R., et al., 2009, *ApJ*, 695, 765
- Meurer G. R., Zheng Z., de Blok W. J. G., 2013, *MNRAS*, 429, 2537
- Miller G. E., Scalo J. M., 1979, *ApJS*, 41, 513
- Minor Q. E., 2013, *ApJ*, 779, 116
- Moffett A. J., et al., 2016, *MNRAS*, 457, 1308
- Momose R., et al., 2013, in Wong T., Ott J., eds, *IAU Symposium Vol. 292, Molecular Gas, Dust, and Star Formation in Galaxies*. pp 335–335
- Muñoz-Mateos J. C., et al., 2009, *ApJ*, 701, 1965
- Oñorbe J., Boylan-Kolchin M., Bullock J. S., Hopkins P. F., Kereš D., Faucher-Giguère C.-A., Quataert E., Murray N., 2015, *MNRAS*, 454, 2092
- Ostriker E. C., McKee C. F., Leroy A. K., 2010, *ApJ*, 721, 975
- Peebles P. J. E., 2017, *Nature Astronomy*, 1, 0057
- Pflamm-Altenburg J., Kroupa P., 2008, *Nature*, 455, 641
- Pflamm-Altenburg J., Kroupa P., 2009, *ApJ*, 706, 516
- Pflamm-Altenburg J., Weidner C., Kroupa P., 2007, *ApJ*, 671, 1550
- Pflamm-Altenburg J., Weidner C., Kroupa P., 2009, *MNRAS*, 395, 394
- Phelps R. L., Janes K. A., 1993, *AJ*, 106, 1870
- Potter A. T., Tout C. A., Eldridge J. J., 2012, *MNRAS*, 419, 748
- Read J. I., Iorio G., Agertz O., Fraternali F., 2017, *MNRAS*, 467, 2019
- Rémy-Ruyer A., et al., 2014, *A&A*, 563, A31
- Riess A., Mack J., 2004, Technical report, Time Dependence of ACS WFC CTE Corrections for Photometry and Future Predictions

- Romano D., Matteucci F., Zhang Z.-Y., Papadopoulos P. P., Iverson R. J., 2017, *MNRAS*, **470**, 401
- Rosenfield P., 2016, padova_tracks: PARSEC + TP-AGB Tracks, doi:10.5281/zenodo.61584
- Roychowdhury S., Chengalur J. N., Begum A., Karachentsev I. D., 2009, *MNRAS*, **397**, 1435
- Roychowdhury S., Huang M.-L., Kauffmann G., Wang J., Chengalur J. N., 2015, *MNRAS*, **449**, 3700
- Ryder S. D., Dopita M. A., 1994, *ApJ*, **430**, 142
- Sacchi E., et al., 2016, *ApJ*, **830**, 3
- Salpeter E. E., 1955, *ApJ*, **121**, 161
- Sanduleak N., 1969, *AJ*, **74**, 877
- Scalo J. M., 1985, in Black D. C., Matthews M. S., eds, Protostars and Planets II. p. 201
- Scalo J. M., 1986, in De Loore C. W. H., Willis A. J., Laskarides P., eds, IAU Symposium Vol. 116, Luminous Stars and Associations in Galaxies. p. p. 451 (S86)
- Scannapieco E., Bildsten L., 2005, *ApJL*, **629**, L85
- Schaerer D., Meynet G., Maeder A., Schaller G., 1993, *AAPS*, **98**, 523
- Schmidt M., 1959, *ApJ*, **129**, 243
- Schneider F. R. N., et al., 2018, *Science*, **359**, 69
- Sirianni M., et al., 2005, *PASP*, **117**, 1049
- Sparre M., Hayward C. C., Feldmann R., Faucher-Giguère C.-A., Muratov A. L., Kereš D., Hopkins P. F., 2017, *MNRAS*, **466**, 88
- Stephens I. W., et al., 2017, *ApJ*, **834**, 94
- Taylor C., Brinks E., Skillman E. D., 1993, *AJ*, **105**, 128
- Taylor C. L., Brinks E., Grashuis R. M., Skillman E. D., 1995, *ApJS*, **99**, 427
- Taylor E. N., et al., 2011, *MNRAS*, **418**, 1587
- Thilker D. A., et al., 2005, *ApJL*, **619**, L79
- Thilker D. A., et al., 2007, *ApJS*, **173**, 538
- Toomre A., 1964, *ApJ*, **139**, 1217
- Tortora C., Napolitano N. R., Cardone V. F., Capaccioli M., Jetzer P., Molinaro R., 2010, *MNRAS*, **407**, 144
- Tremonti C. A., Calzetti D., Leitherer C., Heckman T. M., 2001, *ApJ*, **555**, 322
- Vaughan S. P., Houghton R. C. W., Davies R. L., Zieleniewski S., 2016, preprint (arXiv:1612.00364)
- Verbeke R., De Rijcke S., Koleva M., Cloet-Osselaer A., Vandembroucke B., Schroyen J., 2014, *MNRAS*, **442**, 1830
- Walter F., Brinks E., de Blok W. J. G., Bigiel F., Kennicutt Jr. R. C., Thornley M. D., Leroy A., 2008, *AJ*, **136**, 2563
- Wang J., et al., 2017, *MNRAS*, **472**, 3029
- Watts A., Bekki K., 2016, *MNRAS*, **462**, 3314
- Weidner C., Kroupa P., 2005, *ApJ*, **625**, 754
- Weidner C., Kroupa P., 2006, *MNRAS*, **365**, 1333
- Weidner C., Kroupa P., Maschberger T., 2009, *MNRAS*, **393**, 663
- Weidner C., Kroupa P., Bonnell I. A. D., 2010, *MNRAS*, **401**, 275
- Weisz D. R., et al., 2011, *ApJ*, **739**, 5
- Weisz D. R., Dolphin A. E., Skillman E. D., Holtzman J., Dalcanton J. J., Cole A. A., Neary K., 2013, *MNRAS*, **431**, 364
- Weisz D. R., Dolphin A. E., Skillman E. D., Holtzman J., Gilbert K. M., Dalcanton J. J., Williams B. F., 2015, *ApJ*, **804**, 136
- Williams B. F., et al., 2009a, *AJ*, **137**, 419
- Williams M. J., Bureau M., Cappellari M., 2009b, *MNRAS*, **400**, 1665
- Williams B. F., Dalcanton J. J., Stilp A., Dolphin A., Skillman E. D., Radburn-Smith D., 2013, *ApJ*, **765**, 120
- Wright N. J., Mamajek E. E., 2018, *MNRAS*,
- Wyder T. K., et al., 2009, *ApJ*, **696**, 1834
- Yan Z., Jerabkova T., Kroupa P., 2017, *A&A*, **607**, A126
- Yang W., Meng X., Bi S., Tian Z., Li T., Liu K., 2011, *ApJL*, **731**, L37
- Yorke H. W., Sonnhalter C., 2002, *ApJ*, **569**, 846
- de Blok W. J. G., Walter F., Brinks E., Trachternach C., Oh S.-H., Kennicutt Jr. R. C., 2008, *AJ*, **136**, 2648
- de Vaucouleurs G., de Vaucouleurs A., Corwin Jr. H. G., Buta R. J., Paturel G., Fouqué P., 1991, Third Reference Catalogue of Bright Galaxies. Volume III: Data for galaxies between 12^h and 24^h.
- van Zee L., 2000, *AJ*, **119**, 2757

This paper has been typeset from a \TeX/L\AA\TeX file prepared by the author.